International Journal of Thermal Sciences 118 (2017) 40–52

Contents lists available at ScienceDirect

International Journal of Thermal Sciences

journal homepage: www.elsevier.com/locate/ijts

Constant mass model for the liquid-solid phase transition on a one-dimensional Stefan problem: Transient and steady state regimes

Rubén D. Santiago, Ernesto M. Hernández*, José A. Otero

Tecnológico de Monterrey, Physics Department, Lago de Guadalupe Km. 3.5, Edo. de Mex., 52926 Mexico

ARTICLE INFO

Article history:
Received 12 July 2016
Received in revised form
7 April 2017
Accepted 7 April 2017

Keywords:
Stefan problem
Constant mass
Phase transition

ABSTRACT

One way to study the dynamics of first order phase transitions is through solving the Stefan problem. The goal of this work is to develop a framework that allows researchers to predict the behaviour of a one-dimensional liquid-solid phase transition in the asymptotic time regime by taking into account volumetric effects through mass conservation. In most works on classical Stefan problems, only thermal diffusion in each phase and the variation of the heat flux through the interface by means of the Stefan condition are considered. In this paper, the model is generalized by considering mass conservation as well, which has not been reported before in the literature to the authors knowledge. By using a higher order finite difference scheme and the heat balance integral method for two different types of boundary conditions (isothermal and adiabatic), the improved model is solved.

As a consequence of mass conservation, a subtle change in the thermal balance at the interface (Stefan's condition), is needed. The numerical and semi-analytical solutions for the improved model and the asymptotic values for the interface position, system length, temperature profile and liquid and solid masses, are compared. In the case of isothermal boundary conditions, due to mass conservation, more general asymptotic values are found. A good agreement between the numerical and semi-analytical solutions and the asymptotic time values is observed. In the case of adiabatic boundary conditions, the interface position at thermodynamic equilibrium can be overestimated by the numerical and semi-analytical solutions if only conservation of energy is considered. Finally, by applying mass conservation, a significant error decrease between the numerical and semi-analytical solutions and the predicted values at thermodynamic equilibrium is observed.

1. Introduction

The study of liquid-solid phase transitions has attracted the attention of researchers due to the potential applications of latent heat thermal energy storage (LHTS) systems, which are used to reduce energy consumption demands. In these systems, thermal energy is stored during the melting of a phase change material (PCM) and released during solidification. The thermophysical properties of melting temperature within the desired range of operation, high latent heat of fusion, high thermal conductivity, high specific heat capacity, and small volume changes during the phase transition, make the PCM an ideal candidate for thermal energy storage [1]. The performance of PCM materials in terms of thermal energy storage for building applications, such as PCM wallboard [2], PCM walls [3], PCM ceilings [4], and night cooling for air conditioning applications [5], has been studied. Numerical simulations by genetic algorithms have been used to study the behaviour of a wall with PCM utilizing a simplified model with daily periodic boundary conditions and under real weather data [6]. Experimental characterization of PCM thermophysical properties has also been addressed through the design of energy storage systems where paraffin wax is used as the PCM [7]. Determination of solidification and melting characteristics of paraffin has been done by using energy storage systems. For example, a PCM is stored in an annular space between the inner tube where a heat transfer fluid (HTF) is used [8]. Enhancement of the desired thermophysical properties of PCMs has been reported by using multiwall carbon nanotubes to increase the thermal conductivity of the PCM and reduce the melting/solidification times with little impact on the latent heat of fusion [9].

Numerous works have also been conducted on finding numerical solutions to predict the liquid-solid front (interface) position by

* Corresponding author.
E-mail address: emcooper@itesm.mx (E.M. Hernández).

http://dx.doi.org/10.1016/j.ijthermalsci.2017.04.011
1290-0729/

Nomenclature

ρ_ℓ	Density of liquid phase
ρ_s	Density of solid phase
k_ℓ	Thermal conductivity of the liquid phase
k_s	Thermal conductivity of the solid phase
C_ℓ	Specific heat capacity of the liquid phase
C_s	Specific heat capacity of the solid phase
α	Diffusion constant
L_f	Latent heat of fusion
T_f	Fusion temperature
T_H	Temperature at the right boundary
T_C	Temperature at the left boundary
$\frac{dQ}{dt}$	Heat flux
ΔU	Internal energy change
x_ℓ	Position of the left boundary
x_s	Position of the right boundary
ξ	Interface position
A	Cross section of the one-dimensional rod (system)
L	Initial sample size
M	Total mass of the sample
$x_{\ell_{\text{lim}}}$	Left boundary position in the steady state regime (asymptotic time limit)
$x_{s\ \text{lim}}$	Right boundary position in the steady state regime (asymptotic time limit)
ξ_{lim}	Interface position in the steady state regime (asymptotic time limit)
L_{lim}	Sample size in the steady state regime
$m_{\ell_{\text{lim}}}$	Mass of the liquid phase in the steady state regime
$m_{s_{\text{lim}}}$	Mass of the solid phase in the steady state regime
$x_{\ell_{\text{eq}}}$	Left boundary position at thermodynamic equilibrium
$x_{s_{\text{eq}}}$	Right boundary position at thermodynamic equilibrium
ξ_{eq}	Interface position at thermodynamic equilibrium
L_{eq}	Sample size at thermodynamic equilibrium
$m_{\ell_{\text{eq}}}$	Mass of the liquid phase at thermodynamic equilibrium
$m_{s_{\text{eq}}}$	Mass of the solid phase at thermodynamic equilibrium
M_{eq}	Total mass at thermodynamic equilibrium

using the enthalpy method [10]. Several numerical methods have been used to track the interface position on a finite PCM, such as the fix grid, adaptive mesh, and moving mesh finite difference methods (FDM), where several models for PCMs with packed beds and rectangular, spherical, cylindrical and finned geometry are used [11]. Analytical solutions to the liquid-solid phase transition phenomenon over finite PCMs with different types of boundary conditions have been reported in Refs. [10] and [12]. Cyclic boundary conditions are preferred, since applications of energy storage systems involve exposure to periodic changes of the outside temperature caused by day/night thermal variations [12]. Less work has been done to determine the thermal stress due to the solid-liquid phase transition. A thermomechanical model for a ceramic encapsulated PCM sphere has been proposed [13]. An experimental development of a micro-encapsulated phase change material (MEPCM) with high thermomechanical properties was studied [14], where the voids present in the capsule containing a high fusion temperature PCM compensate for the volume change during the phase transition.

In general, the non linearity introduced in the problem by the moving interface or front has been another factor that has attracted the interest of researchers in studying the dynamics of phase transitions. Since few exact analytical solutions have been presented, a large number of research papers have been devoted to develop numerical strategies to solve these types of problems [11]. Semi-analytical approaches based on the heat balance integral method (HBIM) have been used extensively [15–18] and finite element methods and finite difference methods [19–23] have been used as well. Most of these works verify the consistency of their numerical solutions by comparing them with the few existent exact solutions [19,22,24,25] or solve the problem by using different numerical methods, which are validated through their relative difference. The main disadvantage in using the exact solutions to validate the numerical methods is that they provide information on the interface dynamics for semi-infinite domains. Several works in this field tend to elude finite size effects by comparing their solutions over time domains, where the interface is still within the bulk of the system [24]; some choose the type of boundary conditions that will emulate a semi-infinite system, so the numerical solution shows the classical parabolic behaviour [22], and others use part of the exact solution as a boundary condition [19]. The main focus of all these works has been consistently on the development of more precise, more stable and faster numerical methods. Besides the finite size effects, the impact of thermal dilation and volume changes during the phase transition has been ignored in recent studies [11].

Recently, finite size effects have been taken into account over a one-dimensional system where a liquid-solid phase transition is taking place under homogeneous isothermal or adiabatic boundary conditions [26,27] or under periodic boundary conditions [12]. The position of the interface over large time values (in the steady state regime) may be predicted with the results found in these works. Using heat transport theory [26] and conservation of energy [27], exact analytical expressions can be found for the interface position in the asymptotic time limit. These expressions are frequently used to validate the solutions provided by the numerical and semi-analytical methods.

Although finite size effects have been considered in some works, the effects of volume change during the phase transition must be taken into account. In this work, the effect of the difference in densities between the two phases on the dynamics of the phase transition is studied. The goal of this paper is to extend the model introduced in Refs. [26] and [27] by considering the change in volume during the phase transition and to obtain exact analytical expressions in the steady state regime that are used to validate the numerical and semi-analytical solutions. Therefore, the classical Stefan model is generalized by incorporating the total mass of the system as a constant of the motion. This idea can be extended to non reactive diffusion mechanisms, such as pure iron nitriding [28] [29], and reactive diffusion mechanisms [30], where the interface that separates the two phases that are structurally or chemically different obeys a dynamic behaviour that is governed by the mass balance at the interface position.

This work is organized as follows: in section 2, the model with the thermal diffusion equations at each phase and the thermal balance at the interface is generalized by taking into account the volumetric effects caused by the difference in densities between the two phases. By applying mass conservation, these effects are taken into account. Later in this section, it is also shown that a subtle change must be considered in the equation for the thermal balance at the interface, which is a consequence of mass conservation. At the end of this section, the numerical and semi-analytical

methods used in Refs. [26] and [27] are discussed briefly. In section 3, exact analytical expressions for the asymptotic time behaviour of the interface position, system size and liquid and solid masses are shown. Comparisons of the numerical and semi-analytical solutions with the exact analytical expressions are discussed and illustrated. Finally, in section 4, the main findings are summarized.

2. Model and numerical methods

A finite one-dimensional rod with a liquid-solid interface subject to isothermal and adiabatic boundary conditions is studied in the present work. The thermodynamic variables of thermal conductivity k, specific heat capacity C, and density ρ at each phase are assumed to be constant and do not depend on the temperature. In such a case, the diffusion equation in each phase is reduced to:

$$\frac{\partial T}{\partial t} = \alpha \frac{\partial^2 T}{\partial x^2}, \tag{1}$$

where α is the diffusion constant and is given by $\alpha = k/\rho C$. Two cases are analyzed: a) a rod or system with isothermal boundary conditions, where the left and right boundary of the rod are kept at constant temperature, as shown in Fig. 1:

$$T_\ell(x_\ell, t) = T_{\mathbb{H}}, \text{ and } T_s(x_s, t) = T_{\mathbb{C}}, \tag{2}$$

where $T_{\mathbb{H}}(T_{\mathbb{C}})$ is the temperature at the left(right) boundary located at $x = x_\ell(x = x_s)$ and is above(below) the fusion temperature T_f; b) a rod or system with adiabatic boundary conditions, where the heat flux at each boundary is zero as follows:

$$\frac{\partial T(x,t)}{\partial x}|x = x_\ell = 0, \text{ and } \frac{\partial T(x,t)}{\partial x}|x = x_s = 0. \tag{3}$$

In Ref. [27], it was shown that interface motion is governed by the conservation of energy, and based on this, a relation for the interface position at thermodynamic equilibrium was obtained. This relation was used to predict the amount of liquid and solid that remains in the sample after long time intervals, and these predictions were confirmed by using a fourth-order non-classical finite difference scheme (NC-FDS) along with an approximate analytical solution obtained from the HBIM. The results obtained from the NC-FDS and the HBIM were observed to match the predicted position of the interface at thermodynamic equilibrium, which was obtained by applying conservation of energy:

$$\begin{aligned}\xi_{\text{eq}} &= \frac{\Delta U}{\rho_i L_f} + \xi(0) \text{ where } \Delta U \\ &= \rho_\ell C_\ell \int_{x_\ell}^{\xi(0)} \Big(T_\ell(x,0) - T_f\Big)dx - \rho_s C_s \int_{\xi(0)}^{x_s} \Big(T_f - T_s(x,0)\Big)dx,\end{aligned} \tag{4}$$

where $\xi(0)$ is the initial position of the interface. The coordinates $x_\ell(x_s)$ are shown in Fig. 1, and they represent the position of the left(right) boundaries of the one-dimensional rod; therefore, the length of the rod can be obtained as $L = x_s - x_\ell$. As usual, L_f is the latent heat of fusion, $C_\ell(C_s)$ the specific heat capacities of the liquid(solid), T_f the fusion temperature, and ρ_i is the density of phase i, which may be $\rho_\ell(\rho_s)$, depending on the direction of the phase transition. The variation in energy (ΔU defined as $\Delta U = \Delta U_\ell - \Delta U_s$) is equal to the difference between the energy lost by the liquid and the energy absorbed by the solid phase. It is expressed as an integral of the initial temperature profile $T_\ell(x,0)(T_s(x,0))$ within each phase, and it is equal to the energy used to transform a mass of phase i over a cross-sectional surface A.

A system with a liquid-solid interface is shown in Fig. 1. If the system is subject to adiabatic boundary conditions, the interface position at thermodynamic equilibrium, ξ_{eq}, will be given by equation (4). The initial interface position $\xi(0)$ and temperature profiles $T_\ell(x,0)$ and $T_s(x,0)$, may be chosen so that $\xi_{\text{eq}} < \xi(0)$. This corresponds to a solidification example, where $\rho_i = \rho_s$ should be used in equation (4) to obtain the position of the interface at thermodynamic equilibrium. However, if the interface is very close to x_ℓ at $t = 0$, the variation in the net heat flux is as follows:

$$k_\ell \frac{T_\ell(0,0) - T_f}{\xi(0)} - k_s \frac{T_f - T_s(0,0)}{x_s - \xi(0)} > 0, \tag{5}$$

which will produce melting within the time domain where the above condition is satisfied. This condition is illustrated in Fig. 1a where the heat flux is indicated by the thick arrows. Therefore, the system experiences melting within the first few seconds; however, equation (4) predicts solidification for large time values. This suggests that at some point in time t^*, between the small time regime and the asymptotic time regime, the interface will change its direction of motion.

The behaviour mentioned in the above example is caused by the chosen initial conditions. Therefore, in the time domain where the variation in the heat flux through the interface is positive, that is, for $t < t^*$, ρ_ℓ should be used to obtain the thermal balance at the interface:

$$\rho_\ell L_f \frac{d\xi}{dt} = -k_\ell \frac{\partial T_\ell}{\partial x}|x = \xi + k_s \frac{\partial T_s}{\partial x}|x = \xi, \tag{6}$$

where $k_\ell(k_s)$ is the liquid(solid) thermal conductivity. For times greater than t^*, liquid is transformed into solid, and ρ_s must be used in the equation for the thermal balance at the interface:

$$\rho_s L_f \frac{d\xi}{dt} = -k_\ell \frac{\partial T_\ell}{\partial x}|x = \xi + k_s \frac{\partial T_s}{\partial x}|x = \xi. \tag{7}$$

If the density in the equation for the thermal balance at the interface is changed according to the direction in which the phase transition is taking place, it is found that the solutions obtained with the numerical and semi-analytical methods can considerably overestimate the interface position predicted by equation (4). This is observed because the total mass of the system is not conserved as

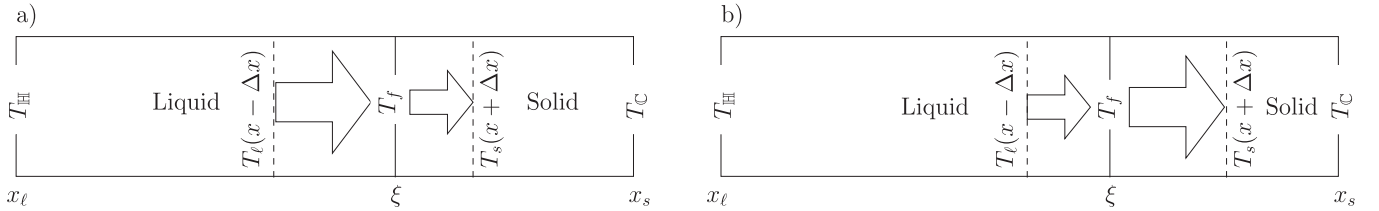

Fig. 1. Schematics of the one-dimensional rod with two phases. a) Example where the heat flux difference causes melting of the solid phase and b) example where the heat flux difference causes formation of the solid phase.

the phase transition takes place.

Typical models of this problem are inconsistent with mass conservation. Inconsistencies between the numerical and semi-analytical solutions and the predicted values are observed because liquid occupies more space than the solid phase, due to its smaller density. Therefore, one way to preserve mass is to change the length of the system as the phase transition is taking place. This will lead to a generalization of the classical Stefan problem by providing an additional differential equation for mass conservation:

$$\rho_\ell A\left(\frac{d\xi}{dt}-\frac{dx_\ell}{dt}\right)+\rho_s A\left(\frac{dx_s}{dt}-\frac{d\xi}{dt}\right)=0, \tag{8}$$

where $x_\ell(x_s)$ is the position of the left(right) boundary of the system, as shown schematically in Fig. 1.

As a consequence of equation (8), there is a subtle change on the equation for the thermal balance at the interface, which will be discussed below. If the substance experiences melting, the interface moves to the right, as shown in Fig. 1a. As seen in this figure, the heat flux in the liquid domain is larger than the heat flux in the solid region. Then, a mass Δm_s, will experience melting on a time interval Δt. The contribution from each phase to the heat flux variation is given by

$$\frac{\Delta Q_\ell}{\Delta t}=k_\ell A\,\frac{T_\ell(\xi-\Delta x,t)-T_\ell(\xi,t)}{\Delta x}\ \text{ and }\ \frac{\Delta Q_s}{\Delta t}=k_s A\,\frac{T_s(\xi,t)-T_s(\xi+\Delta x,t)}{\Delta x}, \tag{9}$$

where $T_\ell(\xi,t)=T_s(\xi,t)=T_f$. If $\Delta Q_\ell/\Delta t>\Delta Q_s/\Delta t$ (the condition for melting), the heat flux variation through the interface when $\Delta t\to 0$ is as follows:

$$\frac{dQ}{dt}=-k_\ell A\,\frac{\partial T_\ell}{\partial x}|x=\xi+k_s A\,\frac{\partial T_s}{\partial x}|x=\xi. \tag{10}$$

During this small time interval, a mass Δm_s of solid will be melted and occupy space as a liquid phase; therefore, the sample will grow according to equation (8). Either boundary can be moved, so assuming first that $dx_\ell/dt\neq 0$ and $dx_s/dt=0$, equation (8) is simplified to:

$$\rho_\ell A\left(\frac{d\xi}{dt}-\frac{dx_\ell}{dt}\right)-\rho_s A\,\frac{d\xi}{dt}=0. \tag{11}$$

The mass of solid Δm_s, which is transformed into liquid over the time interval Δt, is calculated by using the density of the liquid, since it occupies space in its liquid form. Then, for small time intervals, the amount of energy necessary to melt a mass Δm_s of solid is as follows:

$$\frac{dQ}{dt}=\rho_\ell L_f A\left(\frac{d\xi}{dt}-\frac{dx_\ell}{dt}\right). \tag{12}$$

This energy comes from the temperature gradient near the interface, so the equation for the thermal balance at the interface in this case is given by

$$L_f\,\rho_l\left(\frac{d\xi}{dt}-\frac{dx_\ell}{dt}\right)=-k_\ell\,\frac{\partial T_\ell}{\partial x}|x=\xi+k_s\,\frac{\partial T_s}{\partial x}|x=\xi. \tag{13}$$

By the substitution of dx_ℓ/dt from equation (11) in the above expression, equation (7) is obtained. Similar arguments apply when the interface moves to the left (solidification), as shown schematically in Fig. 1b. Here, x_ℓ will move to the right since the transformed liquid occupies less space as a solid. In this case, the heat flux variation through the interface is given by

$$\frac{dQ}{dt}=-k_s A\,\frac{\partial T_s}{\partial x}|x=\xi+k_\ell A\,\frac{\partial T_\ell}{\partial x}|x=\xi, \tag{14}$$

and the mass of liquid transformed into a solid phase is $dm_\ell/dt=-\rho_s A\ d\xi/dt$. Therefore, even if the interface is moving to the left, the thermal balance at $x=\xi$ is exactly the same as shown in equation (7). This is a consequence of mass conservation only. In section 3, when compared with the predicted values at thermodynamic equilibrium, the numerical and semi-analytical solutions are observed to be more consistent for this general model.

If $x=x_s$ is the moving boundary, similar arguments apply. On melting or solidification, the resulting equation for thermal balance at the interface will be given by equation (6). In this case, the results calculated with the NC-FDS and HBIM will also be consistent with the equilibrium values.

2.1. Numerical solutions

The NC-FDS and HBIM used to solve the model just discussed, are fully described in Ref. [26], along with the initial temperature profiles used to solve the problem. A brief description of the generalized NC-FDS, which is applied to a nonhomogeneous moving mesh, is given in this section; however, this method is thoroughly discussed in Ref. [27].

2.1.1. A nonclassical finite difference scheme for a nonhomogeneous moving mesh (NC-FDS)

An implicit scheme is used where the partial time derivative of the temperature is expressed as a first order approximation of the backward difference in time:

$$\frac{\partial T_i}{\partial t}\approx\frac{{}^{m,n}T_i-{}^{m,n-1}T_i}{\Delta t}, \tag{15}$$

where Δt represents the length of the time step. The discretization of the position x is represented by m, and the discretization of time t is represented by n. Therefore, in this notation, ${}^{m,n}T_i=T_i(x_m,t_n)$ in phase i. The generalization of the NC-FDS over a nonhomogeneous mesh is done by adding the Taylor expansions for ${}^{m+1,n}T_i$ and ${}^{m-1,n}T_i$ up to fourth order in Δx_i and by using a step size of different length to the right as $\Delta x_{R_i}={}^{m+1,n}x_i-{}^{m,n}x_i$, and $\Delta x_{L_i}={}^{m,n}x_i-{}^{m-1,n}x_i$ to the left.

In the expression that results from the addition of these Taylor expansions, some terms appear with the third and fourth derivatives in x that may be conveniently expressed in terms of second order derivatives. The discretized heat equation is substituted in every term with a second order derivative, and after simplification of the remaining expression, the following 6-point model is obtained:

$$\left(\gamma_i^{(L)}-\lambda_i^{(L)}\right){}^{m-1,n}T_i+\left(2\lambda_i+\frac{5}{6}\right){}^{m,n}T_i+\left(\gamma_i^{(R)}-\lambda_i^{(R)}\right){}^{m+1,n}T_i=\gamma_i^{(L)}\,{}^{m-1,n-1}T_i+\frac{5}{6}\,{}^{m,n-1}T_i+\gamma_i^{(R)}\,{}^{m+1,n-1}T_i,{}^{m+1,n-1}T_i \tag{16}$$

where the following expressions have been defined:

$$\lambda_i=\frac{\alpha_i\Delta t}{\Delta x_{R_i}\Delta x_{L_i}},\ \lambda_i^{(L)}=\frac{2\alpha_i\Delta t}{\Delta x_{L_i}(\Delta x_{R_i}+\Delta x_{L_i})},\ \lambda_i^{(R)}=\frac{2\alpha_i\Delta t}{\Delta x_{R_i}(\Delta x_{R_i}+\Delta x_{L_i})},$$

and

$$\gamma_i^{(L)} = \frac{2\Delta x_{L_i} - \Delta x_{R_i}}{6(\Delta x_{R_i} + \Delta x_{L_i})},\ \gamma_i^{(R)} = \frac{2\Delta x_{R_i} - \Delta x_{L_i}}{6(\Delta x_{R_i} + \Delta x_{L_i})}.$$

The fourth order approximation to the derivatives that appear in equation (3) for adiabatic boundary conditions and in the thermal balance at the interface, equations (6) and (7), is given by

$$^{m,n}T_S{}^{(1)} = \frac{1}{12\Delta x_{R_s}}(-25\,{}^{m,n}T_s + 48\,{}^{m+1,n}T_s - 36\,{}^{m+2,n}T_s + 16\,{}^{m+3,n}T_s - 3\,{}^{m+4,n}T_s), \quad (17)$$

and

$$^{m,n}T_\ell{}^{(1)} = \frac{1}{12\Delta x_{L_\ell}}(25\,{}^{m,n}T_\ell - 48\,{}^{m-1,n}T_\ell + 36\,{}^{m-2,n}T_\ell - 16\,{}^{m-3,n}T_\ell + 3\,{}^{m-4,n}T_\ell). \quad (18)$$

These fourth order approximations to the first derivative that appears in the thermal balance at the interface are used to obtain an estimate of the interface position. The estimated interface position at time $t + \Delta t$, which is written in this notation as ${}^{n+1}\xi$, is used to calculate the position of the moving boundary by using mass conservation. For all the calculations done with the NC-FDS, conservation of mass is imposed as follows:

$$\rho_\ell(\xi(t) - x_\ell(t)) + \rho_s(x_s(t) - \xi(t)) = \rho_\ell(\xi(t+\Delta t) - x_\ell(t+\Delta t)) + \rho_s(x_s(t+\Delta t) - \xi(t+\Delta t)). \quad (19)$$

Therefore, if x_ℓ is the moving boundary, its new position is calculated as follows:

$${}^{n+1}x_\ell = {}^{n}x_\ell - \left(\frac{\rho_s}{\rho_\ell} - 1\right)({}^{n+1}\xi - {}^{n}\xi), \quad (20)$$

if x_s is the time-dependent boundary, according to mass conservation, the discretized equation of motion is given by

$${}^{n+1}x_s = {}^{n}x_s + \left(1 - \frac{\rho_\ell}{\rho_s}\right)({}^{n+1}\xi - {}^{n}\xi). \quad (21)$$

2.1.2. Approximate analytical solution

This method is based on the HBIM of Goodman, where temperature profiles are assumed to be parabolic functions in the position; however, higher-order polynomials can be considered [27]. The approximate analytical solution described in Refs. [26] and [27] is extended to the model presented in this work, where the temperature profiles are given by

$$T_\ell(x,t) = a_\ell(\xi - x) + b_\ell(\xi - x)^2 + T_f,\ \text{with}\ x_\ell \le x \le \xi, \quad (22)$$

for the liquid phase, and

$$T_\ell(x,t) = a_s(x - \xi) + b_s(x - \xi)^2 + T_f,\ \text{with}\ \xi \le x \le x_s \quad (23)$$

for the solid phase, where $a_\ell(a_s)$ and $b_\ell(b_s)$ are functions of time that belong to the temperature profile in the liquid(solid) phase. The value of these functions at $t = 0$ s can be determined from the boundary conditions given by equation (2) for isothermal boundary conditions or equation (3), for adiabatic boundary conditions.

The time behaviour of the interface is obtained by substituting these profiles in the equation for the thermal balance at the interface. If x_ℓ is the time-dependent boundary and x_s is constant, the temperature profiles must be substituted in equation (7). The resulting equation is an ordinary differential equation in time (ODE) for ξ. Similarly, if x_ℓ is constant and x_s depends on time, the resulting ODE can be obtained by substituting the temperature profiles in equation (6). In addition, mass conservation is imposed by using equation (8), which is already an ODE in time. If x_s is constant, mass conservation is reduced to equation (11). If x_ℓ is kept constant, equation (8) is reduced as follows:

$$\rho_\ell A \frac{d\xi}{dt} + \rho_s A\left(\frac{dx_s}{dt} - \frac{d\xi}{dt}\right) = 0. \quad (24)$$

Finally, the temperature profiles given by equations (22) and (23) must be substituted in the diffusion equation for each phase, equation (1), and averaged over the position variable, by integrating the resulting equations from $x = x_\ell$ to $x = \xi$ in the liquid phase and from $x = \xi$ to $x = x_s$ in the solid phase. The two equations obtained from this process, along with the thermal balance at the interface, equation (6) or (7) and mass conservation, equation (11) or (24), constitute a set of four ODEs in time, which is solved for the position of the interface, the temperature profile at each phase and the position of the time-dependent boundary x_ℓ or x_s.

3. Results and discussion

In this section, a general expression for the asymptotic time limit of the interface position in a system with isothermal boundary conditions is obtained. The left and right boundaries are kept at constant temperature $T_\ell(x_\ell, t) = T_H$ and $T_s(x_s, t) = T_C$, due to a heat bath and a cold reservoir, as shown in Fig. 1. The interface will move to a position $\xi_{\lim}$ where the variation in the heat flux becomes zero:

$$k_\ell A \frac{T_H - T_f}{\xi_{\lim} - x_{l_{\lim}}} = k_s A \frac{T_f - T_C}{x_s - \xi_{\lim}}, \quad (25)$$

where $x_{\ell_{\lim}}$ is the position of the left boundary in this limit (the other boundary is assumed to be fixed in time). Mass conservation can be applied as follows:

$$\rho_\ell A\,(\xi_{\lim} - x_{\ell_{\lim}}) + \rho_s A\,(x_s - \xi_{\lim}) = \rho_\ell A\,(\xi(0) - x_\ell(0)) + \rho_s A\,(x_s - \xi(0)), \quad (26)$$

where the left-hand side is the total mass for large time values and the right-hand side is the total mass at $t = 0$. The value of $\xi_{\lim}$ can be obtained from the last two equations as follows:

$$\xi_{\lim} = \frac{\rho_\ell k_\ell \left(T_H - T_f\right) x_s + k_s \left(T_f - T_C\right)(\rho_\ell x_\ell(0) + (\rho_s - \rho_\ell)\xi(0))}{\rho_\ell k_\ell \left(T_H - T_f\right) + \rho_s k_s \left(T_f - T_C\right)}. \quad (27)$$

In the previous equation, time dependence is shown explicitly in the moving boundary, $x_\ell(0)$, while x_s is constant.

The length of the system, $L_{\lim} = x_s - x_{\ell_{\lim}}$, can be obtained with the following equation:

$$L_{\lim} = \frac{\left(k_\ell \left(T_H - T_f\right) + k_s \left(T_f - T_C\right)\right)(\rho_s x_s - \rho_\ell x_\ell(0) - (\rho_s - \rho_\ell)\xi(0))}{\rho_\ell k_\ell \left(T_H - T_f\right) + \rho_s k_s \left(T_f - T_C\right)}. \quad (28)$$

If instead, x_s is the time-dependent boundary, the interface position in the asymptotic time limit can be obtained in a similar way as follows:

$$\xi_{\lim} = \frac{\rho_s\, k_s \left(T_f - T_{\mathrm{C}}\right) x_l + k_\ell \left(T_{\mathrm{H}} - T_f\right) \left(\rho_s\, x_s(0) - \left(\rho_s - \rho_\ell\right) \xi(0)\right)}{\rho_\ell\, k_\ell \left(T_{\mathrm{H}} - T_f\right) + \rho_s\, k_s \left(T_f - T_{\mathrm{C}}\right)}. \tag{29}$$

Equations (27) and (29) predict a different position in this limit because these equations give the coordinate of the interface relative to the chosen frame of reference. However, the length of the sample should not depend on the reference frame, which means that equation (28) is valid, regardless of which boundary is free to move. Using mass conservation and equation (29), it is straightforward to show that equation (28) still holds when x_s is the time-dependent boundary. The resulting expressions that appear in equations (27) and (29) are a generalization of the results presented in Refs. [12] and [26], where the sample size was constant in time and the interface position in the asymptotic limit was found to be

$$\xi_{\lim} = \frac{k_\ell \left(T_{\mathrm{H}} - T_f\right)}{k_\ell \left(T_{\mathrm{H}} - T_f\right) + k_s \left(T_f - T_{\mathrm{C}}\right)} L. \tag{30}$$

If the densities in each medium are equal, which can be done by setting $\rho_\ell = \rho_s$ in equations (27) and (29), and $x_\ell = 0$, equation (30) is recovered. In Ref. [12], equation (30) represents the steady state component of the solution for a system with boundary conditions that are periodic in time. It is the same expression found in Ref. [26], where this result is used to design cases where the predictive power of equation (30) is illustrated for a system with isothermal boundary conditions.The time behaviour of the interface is best described in terms of the mass because this physical quantity should not depend on the chosen frame of reference; therefore, liquid and solid masses can be shown to behave asymptotically as

$$\begin{aligned} m_{\ell_{\lim}} &= \left(\frac{\rho_\ell k_\ell \left(T_{\mathrm{H}} - T_f\right) M}{\rho_\ell k_\ell \left(T_{\mathrm{H}} - T_f\right) + \rho_s k_s \left(T_f - T_{\mathrm{C}}\right)}\right) \text{ and } m_{s_{\lim}} \\ &= \left(\frac{\rho_s k_s \left(T_f - T_{\mathrm{C}}\right) M}{\rho_\ell k_l \left(T_{\mathrm{H}} - T_f\right) + \rho_s k_s \left(T_f - T_{\mathrm{C}}\right)}\right), \end{aligned} \tag{31}$$

where M is the total mass of the system. Equation (31) is obtained, whether x_ℓ or x_s is chosen as the moving boundary.

For all the examples discussed below, the thermodynamic variables are taken from Ref. [22], all quantities are calculated by using the mks system of units, and mass values are obtained from a rod with one square unit of cross section. In Fig. 2, the dynamics of the interface for aluminum is shown. The left(right) boundaries are kept at 1100K(820K), and the fusion point of aluminum is taken as $T_f = 933.52$K. The initial length of the system is $L(0) = 1$m, and the initial position is chosen as $\xi(0\text{s}) = 0.80$m so that only the formation of the solid phase is observed. The results from this example are illustrated in Fig. 2, where the time behaviour of the right and left boundary of the sample is calculated by using mass conservation. Fig. 2a shows in solid lines the solution calculated with the numerical and semi-analytical methods by moving the right boundary x_s, along with the asymptotic interface position according to equation (29). The result obtained by moving the left boundary x_ℓ, along with the asymptotic time limit according to equation (27), is shown in dotted lines. In Fig. 2b, the resulting time behaviour of L and its corresponding asymptotic limit is also shown. It is observed that in both cases, the time behaviour of L is the same and both have the same asymptotic time limit as predicted by equation (28). Finally, in Fig. 2c, d and 2e, the total mass of the sample M and the mass of the liquid and solid phases obtained from the NC-FDS and HBIM are shown, along with the corresponding asymptotic values from equation (31). As observed, the time evolution of the liquid and solid masses does not depend on which boundary is chosen to move and has the same asymptotic time limit as predicted by equation (31).

Melting of the solid can be observed by changing only the initial interface position of the previous example. This is shown in Fig. 3, where the initial position of the interface is $\xi(0\text{s}) = 0.20$m, whereas all remaining variables have the same values as in Fig. 2. In this example, the numerical and semi-analytical results obtained by moving the left boundary and the corresponding asymptotic time limit for the interface position according to equation (27) and the asymptotic limits according to equations (28) and (31) appear with solid lines. The results obtained by moving the right boundary and the corresponding asymptotic time limits for the interface position according to equation (29) and system length and liquid and solid masses according to equations (28) and (31) are shown in dotted lines.

For this type of boundary conditions, it is also found in Refs. [12] and [26] that the temperature along the entire sample has an exact asymptotic expression for a system with constant length. The temperature profile for large time values can be obtained, not only because the heat flux variation is zero at the interface, but also because the net heat flux vanishes at any point within the sample. This means that the asymptotic temperature profile, which is found in Refs. [12] and [26] for the particular case of a system with constant length, also has a more general form when mass conservation is taken into account. Since the net heat flux at any point within the liquid and solid phases is zero, the following equation must be satisfied at any position along the liquid domain:

$$\frac{T_{\mathrm{H}} - T_\ell^{\lim}(x)}{x - x_{\ell_{\lim}}} = \frac{T_\ell^{\lim}(x) - T_f}{\xi_{\lim} - x} \text{ for } x_{\ell_{\lim}} < x < \xi_{\lim}, \tag{32}$$

where $T_\ell^{\lim}(x)$ is the temperature profile within the liquid, in the asymptotic time limit. Similarly, the following equation must be satisfied for the solid phase:

$$\frac{T_f - T_s^{\lim}(x)}{x - \xi_{\lim}} = \frac{T_s^{\lim}(x) - T_{\mathrm{C}}}{x_s - x} \text{ for } \xi_{\lim} < x < x_s, \tag{33}$$

with $T_s^{\lim}(x)$ being the temperature profile within the solid phase in this limit. Solving for $T_\ell^{\lim}(x)$ and $T_s^{\lim}(x)$ from the above equations and using equation (27), which is obtained when the left boundary is allowed to move, a general expression for the temperature profile in the asymptotic limit can be obtained for the liquid phase as follows:

$$T_\ell^{\lim}(x) = T_f + \frac{\rho_\ell\, k_\ell \left(T_{\mathrm{H}} - T_f\right) \left(x_s - x\right) + k_s \left(T_f - T_{\mathrm{C}}\right) \left(\rho_s \left(\xi(0) - x\right) - \rho_\ell \left(\xi(0) - x_\ell(0)\right)\right)}{k_\ell\, M} \tag{34}$$

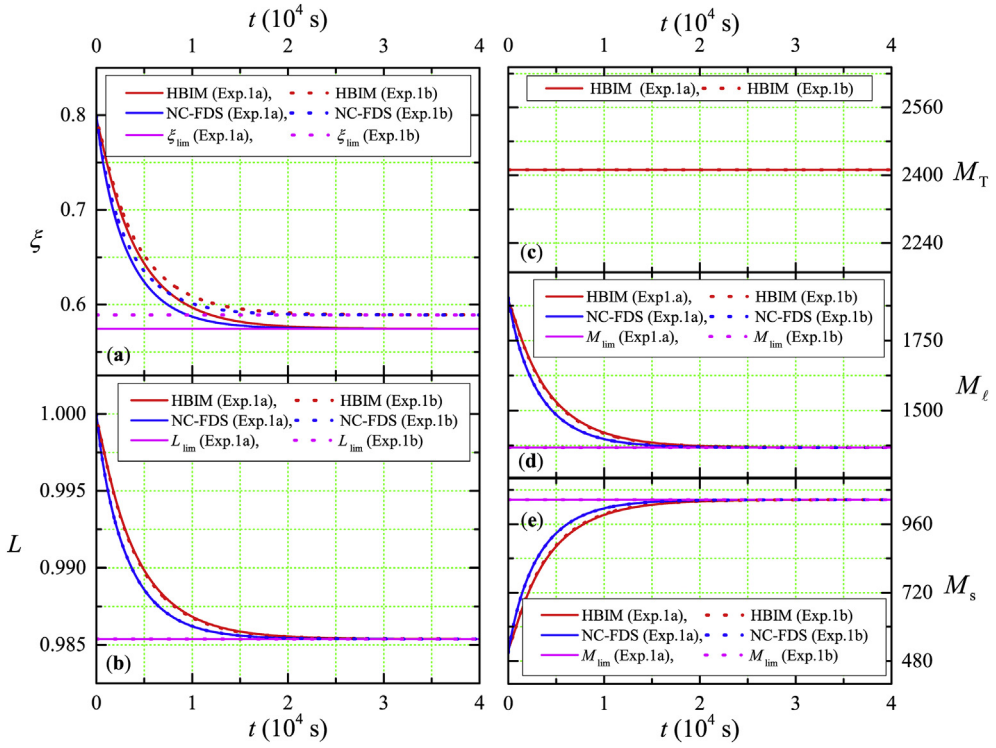

Fig. 2. NC-FDS, HBIM solutions, and corresponding asymptotic values for a) interface position, b) L, c) total mass, d) liquid phase mass, and e) solid phase mass. Experiment 1a is shown in solid lines, where the time-dependent boundary is x_s, and experiment 1b is shown in dotted lines, where the time-dependent boundary is x_ℓ.

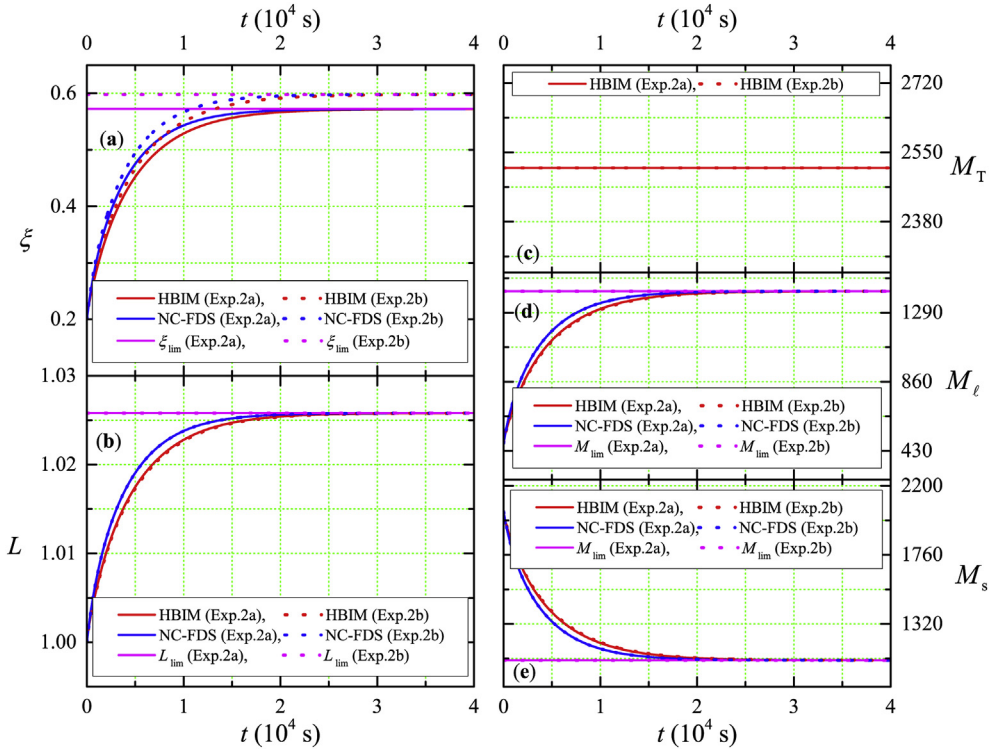

Fig. 3. Experiment 2a shows in solid lines the NC-FDS, HBIM solutions, and corresponding asymptotic values from equations (27), (28) and (31) for the interface position, sample size, and mass when the left boundary is allowed to move. In dotted lines, experiment 2b shows the numerical and semi-analytical solutions and corresponding asymptotic values, according to equations (28), (29) and (31), when the right boundary moves in time.

and in the solid phase:

$$T_s^{\lim}(x) = T_{\mathrm{C}} + \frac{\rho_\ell\, k_\ell \left(T_{\mathrm{H}} - T_f\right) + \rho_s\, k_s \left(T_f - T_{\mathrm{C}}\right)}{k_s\, M}\,(x_s - x). \quad (35)$$

In the same manner, for a system with constant length, the asymptotic temperature profiles found in Refs. [12] and [26], can be obtained by substitution of $\xi_{\lim}$ from equation (30), in equations (32) and (33).

If the right boundary is allowed to move and the other boundary is fixed, the asymptotic temperature profile can be obtained by using the interface position from equation (29). Therefore, the temperature profile within the liquid phase, is given by

$$T_\ell^{\lim}(x) = T_{\mathrm{H}} - \frac{\rho_\ell\, k_\ell \left(T_{\mathrm{H}} - T_f\right) + \rho_s\, k_s \left(T_f - T_{\mathrm{C}}\right)}{k_\ell\, M}\,(x - x_\ell), \quad (36)$$

and for the solid phase, the following is obtained:

$$T_s^{\lim}(x) = T_f - \frac{\rho_s\, k_s \left(T_f - T_{\mathrm{C}}\right)(x - x_\ell) + k_\ell \left(T_{\mathrm{H}} - T_f\right)\left(\rho_\ell\,(x - \xi(0)) - \rho_s\,(x_s(0) - \xi(0))\right)}{k_s\, M}. \quad (37)$$

Equations (34) and (35) predict a different temperature profile to that obtained by using equations (36) and (37) because these expressions depend on the frame of reference. In Fig. 4, the time evolution of the temperature profiles $T_\ell(x,t)$ and $T_s(x,t)$ is illustrated for a system where x_ℓ moves in time and x_s is constant. The initial conditions used to build this figure are obtained from the example shown in Fig. 3. The asymptotic temperature profile, calculated from equations (34) and (35), is shown and compared with the semi-analytical solution obtained from the HBIM. The agreement between the HBIM and equations (34) and (35) show that these solutions are consistent with the predicted physical behaviour and provide exact analytical expressions that describe the dynamics of the phase transition in the asymptotic time limit.

When the nature of the boundary conditions is changed, the time behaviour of the interface is completely different. If the system is thermally isolated, there are cases where the initial conditions (interface position and temperature profiles) may be chosen so that the interface position changes its direction of motion at some time t^*, as described in section 2. Assuming first that after long time intervals, some of the solid will be transformed into liquid phase, the values of all the dynamic variables at thermodynamic equilibrium, will be obtained by using energy and mass conservation. Equilibrium values for ξ_{eq} and $x_{\ell_{\mathrm{eq}}}$, where x_ℓ is chosen to be the time-dependent boundary, are given by

$$\xi_{\mathrm{eq}} = \frac{\Delta U}{\rho_s\, L_f} + \xi(0) \;\text{ and }\; x_{\ell_{\mathrm{eq}}} = \left(\frac{1}{\rho_s} - \frac{1}{\rho_\ell}\right)\frac{\Delta U}{L_f} + x_\ell(0). \quad (38)$$

The only difference with equation (4) is the density being used to calculate the equilibrium value. Using the density of the solid phase to obtain the interface position at thermodynamic equilibrium could be counterintuitive, because for large time values, the

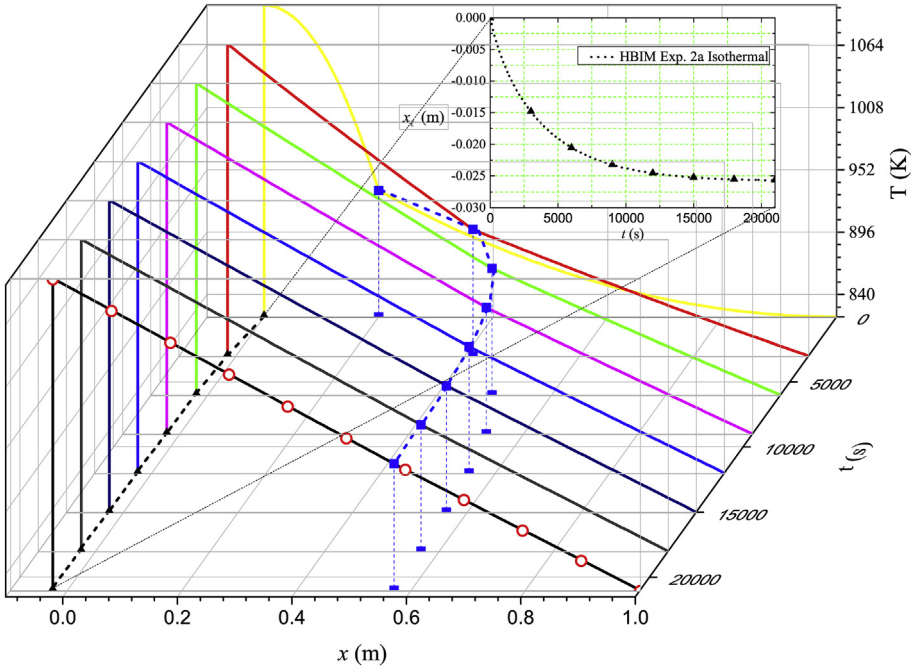

Fig. 4. Temperature profiles at different time values, calculated for experiment 2a (illustrated in Fig. 3) with the semi-analytical method (HBIM). The corresponding asymptotic behaviour according to equations (34) and (35) is shown in white circles. The interface and the left boundary positions are also shown in blue squares and black triangles, respectively. For a better appreciation, the inset shows the time evolution of the left boundary in the domain $x_{\ell_{\lim}} < x < 0$. (For interpretation of the references to colour in this figure legend, the reader is referred to the web version of this article.)

melted solid occupies space in its liquid form. Nevertheless, the density that is used in equation (38) for ξ_{eq} is a consequence of mass conservation and of choosing x_ℓ as the moving boundary. From equation (38), the length of the system at thermodynamic equilibrium can be found as follows:

$$L_{eq} = x_s - x_\ell(0) + \left(\frac{1}{\rho_\ell} - \frac{1}{\rho_s}\right)\frac{\Delta U}{L_f}. \tag{39}$$

If x_s is chosen to move and x_ℓ is constant, ξ_{eq} and $x_{s_{eq}}$ are given by

$$\xi_{eq} = \frac{\Delta U}{\rho_\ell L_f} + \xi(0) \text{ and } x_{s_{eq}} = x_s(0) + \left(\frac{1}{\rho_\ell} - \frac{1}{\rho_s}\right)\frac{\Delta U}{L_f}, \tag{40}$$

which is different to the value predicted by equation (38) simply because ξ is a quantity that depends on the reference frame. It can be seen from equation (40) that the expression for L_{eq} appearing in equation (39) is recovered, as it should be, given that L does not depend on the frame of reference. If the formation of the solid phase is expected after the system reaches thermodynamic equilibrium, the situation can be analyzed in a similar way. The sample will decrease in size according to equation (39), and ξ_{eq} will still satisfy equations (38) and (40), depending on which boundary is moved. Finally, the mass of each phase can be obtained as follows:

$$m_{\ell_{eq}} = \rho_\ell(\xi(0) - x_\ell(0)) + \frac{\Delta U}{L_f} \text{ and } m_{s_{eq}} = \rho_s(x_s(0) - \xi(0)) - \frac{\Delta U}{L_f}. \tag{41}$$

In Fig. 5, a solidification example is shown for an aluminum rod of constant length ($L = 1$m), where the initial temperature profile and interface position were chosen to observe melting within the small time regime and solidification as the system approaches thermodynamic equilibrium. The initial temperature of the left(-right) boundary and initial interface position are.

$T_\ell(0,0) = 1170\text{K}(T_s(x_s,0) = 820.25\text{K})$ and $\xi(0) = 0.20$m, respectively. The most interesting aspect of Fig. 5 is that both methods considerably overestimate the value of ξ_{eq} obtained from equation (4). The mass of the liquid and solid phases at thermodynamic equilibrium can be calculated by using equation (4), when the length of the system is constant, as follows:

$$m_{\ell_{eq}} = \rho_\ell\left(\frac{\Delta U}{\rho_i L_f} + \xi(0)\right) \text{ and } m_{s_{eq}} = \rho_s\left(L - \frac{\Delta U}{\rho_i L_f} - \xi(0)\right), \tag{42}$$

and the total mass will change in time, approaching asymptotically to

$$M_{eq} = (\rho_\ell - \rho_s)\left(\frac{\Delta U}{\rho_i L_f}\right) + M(0), \tag{43}$$

where $M(0)$ is the initial mass of the system, $M(0) = \rho_\ell\,\xi(0) + \rho_s\,(L - \xi(0))$.

By using the constant mass model, the inconsistencies shown in Fig. 5 can be corrected. The results obtained with the numerical and semi-analytical methods are shown in Fig. 6. Experiment 1a in this figure, shows in solid lines the solutions obtained by assuming that x_s moves in time and x_ℓ is constant. Experiment 1b shows in dotted lines the solutions calculated by assuming that x_s is constant and x_ℓ is moving in time. In Fig. 6a, the calculated value of ξ, labeled as experiment 1a and shown in solid lines, approaches the equilibrium position given by equation (40). The result for ξ, labeled as

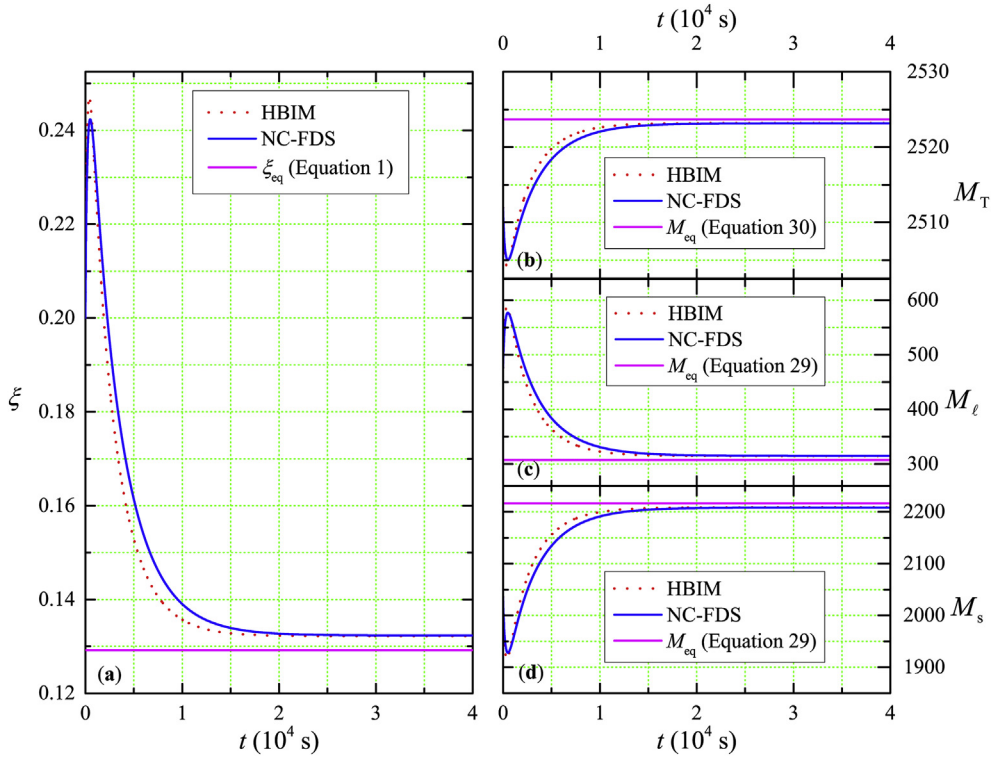

Fig. 5. NC-FDS and HBIM solutions for the a) interface position, b) total mass, c) liquid mass, and d) solid mass. A comparison with the corresponding values at thermodynamic equilibrium, according to equations (4), (42) and (43), is also shown. The interface position and the mass of each phase, calculated with the NC-FDS and HBIM, deviate significantly from the equilibrium values.

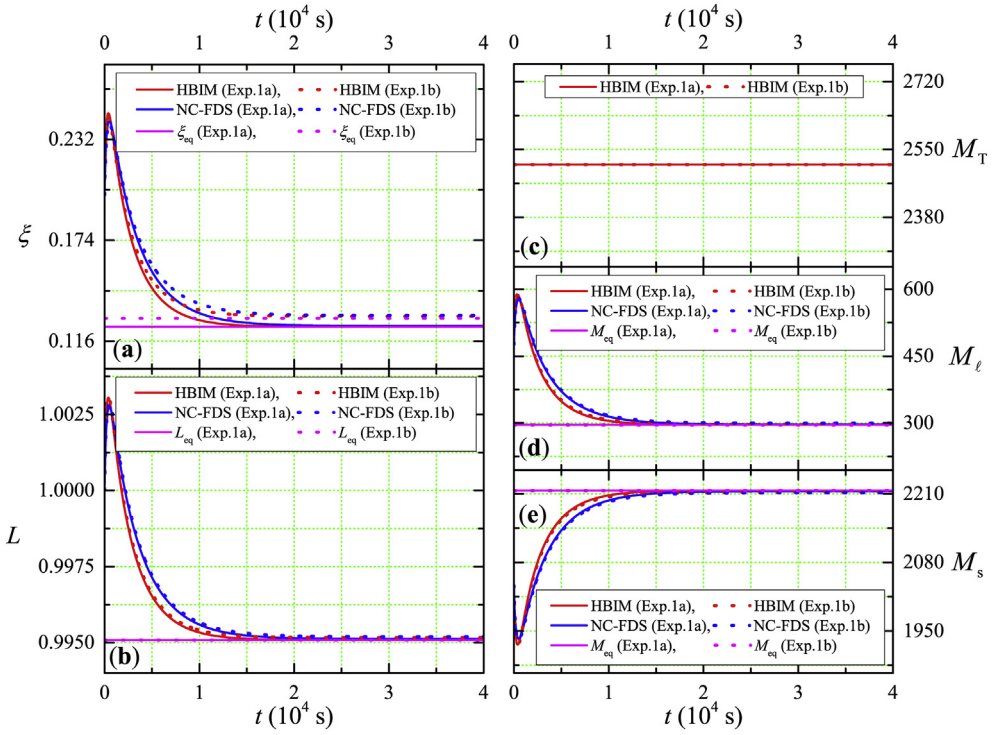

Fig. 6. Time evolution for the a) interface position, b) sample length, c) total mass and d) liquid and e) solid masses corresponding to the example shown in Fig. 5. Experiment 3a is shown in solid lines and corresponds to the case where x_s depends on time and x_ℓ is constant. Experiment 3b is shown in dotted lines and corresponds to a system where x_s is constant and x_ℓ moves in time.

experiment 1b and shown in dotted lines, approaches the equilibrium position predicted by equation (38), when x_ℓ moves in time and x_s is constant. In both experiments, the results obtained from the HBIM and the NC-FDS approach to the asymptotic values with less error than the one observed for a system with constant length. The error between these results and ξ_{eq} decreases significantly when compared to the error observed in Fig. 5. Fig. 6b, c, 6d, and 6e show the time evolution for the system length, total mass and liquid and solid masses, respectively. In each experiment, the time evolution obtained for these variables is the same, given that they should not depend on the frame of reference, and approach the same equilibrium values given by equations (39) and (41). The errors between the equilibrium values for the liquid and solid masses and the numerical estimates also decrease significantly by using the improved model.

The percentage errors corresponding to experiment 1a are shown in Table 1, where the numerical and semi-analytical solutions at $t = 4 \times 10^4$ s are compared with the exact equilibrium values obtained from equation (40) for the interface position and equation (41) for the liquid and solid masses. In Table 1, the equilibrium values obtained from the example shown in Fig. 5 are also shown. The percentage errors for the interface position and liquid

Table 1
Percent relative difference between values calculated with the HBIM and the NC-FDS at $t = 1 \times 10^4$ s, and the exact values at thermodynamic equilibrium obtained from the example shown in Figs. 5 and 6. Percent relative differences were calculated as $\left|(Y^{T}_{eq} - Y^{num}_{eq})/Y^{T}_{eq}\right| \times 100\%$.

Model	ξ^{T}_{eq}	ξ^{HBIM}_{eq}	ξ^{NC-FDS}_{eq}	HBIM Error	NC-FDS Error
	m	m	m	%	%
Constant Length	0.1291476	0.1321939	0.1323440	2.3587978	2.4749976
Constant Mass Exp. 1a	0.1242355	0.1242381	0.1247941	0.0020928	0.4496299
Constant Mass Exp. 1b	0.1291476	0.1303094	0.1307288	0.8995909	1.2243356
	$m^{T}_{\ell_{eq}}$	$m^{HBIM}_{\ell_{eq}}$	$m^{NC-FDS}_{\ell_{eq}}$	HBIM Error	NC-FDS Error
	kg	kg	kg	%	%
Constant Length	307.37122	314.62159	314.97874	2.3588318	2.4750268
Constant Mass Exp. 1a	295.68057	295.68672	297.01000	0.0020799	0.4496170
Constant Mass Exp. 1b	295.68057	298.63754	299.70472	1.0000560	1.3609788
	$m^{T}_{s_{eq}}$	$m^{HBIM}_{s_{eq}}$	$m^{NC-FDS}_{s_{eq}}$	HBIM Error	NC-FDS Error
	kg	kg	kg	%	%
Constant Length	2216.3194	2208.5664	2208.1845	0.3498142	0.3670455
Constant Mass Exp. 1a	2216.3194	2216.3133	2214.9900	0.0002752	0.0599823
Constant Mass Exp. 1b	2216.3194	2213.3625	2212.2953	0.1334149	0.1815668

and solid masses are obtained by comparing the exact equilibrium values from equations (4) and (42) with the calculated numerical and semi-analytical values at $t = 4 \times 10^4$s, for a system with constant length. In the case of the HBIM solutions, it can be observed that errors obtained with the constant mass model in experiment 1a are approximately 10^3 orders of magnitude smaller than the relative errors observed for the system with constant length. Even more, the relative errors calculated with the NC-FDS solutions are observed to be about 6–7 times smaller for experiment 1a, compared to the calculated errors for the system with constant length. The relative errors obtained for experiment 1b are also shown in Table 1. In this numerical experiment, where x_ℓ is free to move, the relative errors are obtained by using the equilibrium values from equation (38) for the interface position and equation (41) for the liquid and solid masses. In this case, however, the improvement is less drastic, and the calculated relative errors from the HBIM values of experiment 1b decrease at most by a factor of 3 and by a factor of 2 for the NC-FDS, when compared with the errors for the system with constant length.

The last example is shown in Figs. 7 and 8. The initial temperatures on the left (right) boundary and initial interface position are $T_\ell(0,0) = 1000\text{K}(T_s(x_s,0) = 820.25\text{K})$ and $\xi(0) = 0.80\text{m}$, respectively. By placing more liquid than solid phase within the system, more internal energy is available, so overall melting is expected according to equation (4). The situation for a system of constant length is shown in Fig. 7, where the numerical and semi-analytical solutions significantly overestimate the values predicted by equations (4) and (42).

Finally, this example was modeled by using mass conservation. In Fig. 8, the solid lines correspond to a system where x_s is constant and x_ℓ is the time-dependent boundary. The dotted lines in this figure show the results obtained for a system where x_s is moving in time and x_ℓ is constant. As illustrated in Fig. 8 and Table 2, the difference between the numerical and semi-analytical solutions and the equilibrium values given by equations (38), (40) and (41) is significantly reduced. For experiment 2a, where x_ℓ is moving in time, the errors calculated from the HBIM are reduced approximately by a factor of 50 times, compared with the errors calculated from the constant length model. The errors obtained from the NC-FDS are reduced approximately by a factor of 5. For experiment 2b, where x_s is the time-dependent boundary, the errors obtained from the HBIM are decreased by a factor of 20, whereas for the NC-FDS, these errors are reduced by a factor of 100, when compared with the errors calculated from the constant length system shown in Fig. 7.

4. Conclusions

The goal of this work was twofold: first, to obtain a more general model for the one-dimensional Stefan problem, where the change in volume during the phase transition is taken into account, and second, to show exact analytical expressions in the asymptotic time limit that consider these volumetric effects.

It has been shown that, considering liquid and solid phases with different densities and in the case in which the phase transition takes place in both directions, the classical model of the Stefan problem is ill-defined. This is because the predictions of the interface position at thermodynamic equilibrium are overestimated by the numerical and semi-analytical solutions. This lead to a generalization of the Stefan problem with the following results:

- The classical model was extended by adding mass conservation, which takes into account the difference in densities between both phases.
- Subtle changes in the Stefan condition were needed, and it is shown that these changes are a consequence of mass conservation only.

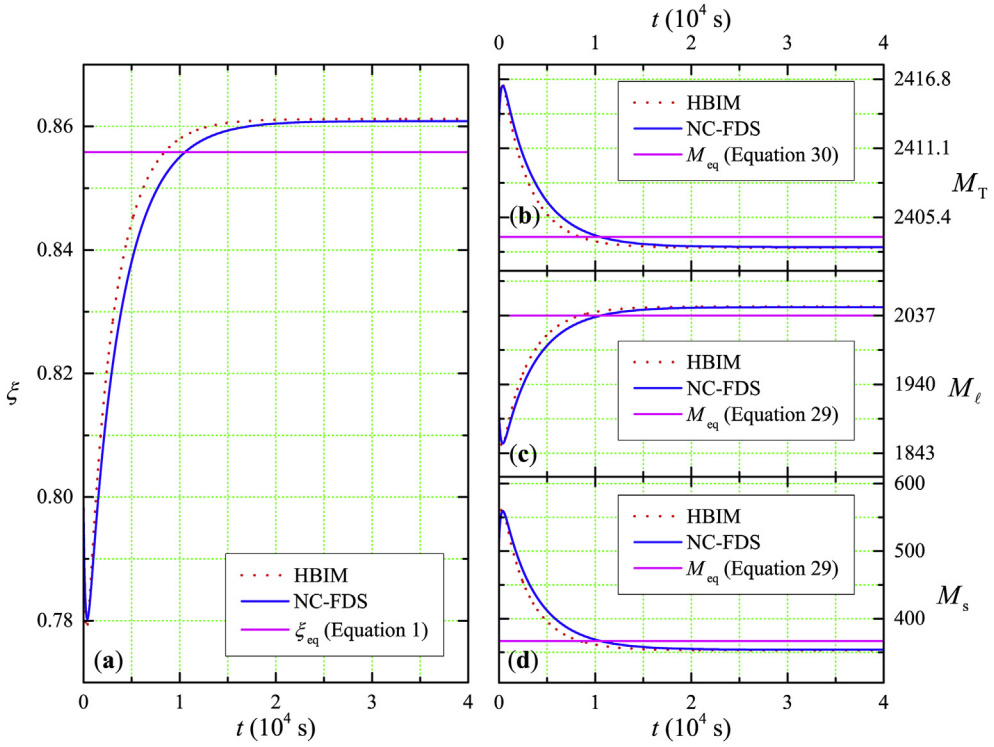

Fig. 7. Solutions from the NC-FDS and HBIM along with the corresponding equilibrium values for the a) interface position, b) total mass and c) liquid and d) solid masses for a system of constant length. This figure shows the inconsistencies between the values at thermodynamic equilibrium and the solutions obtained with the HBIM and NC-FDS.

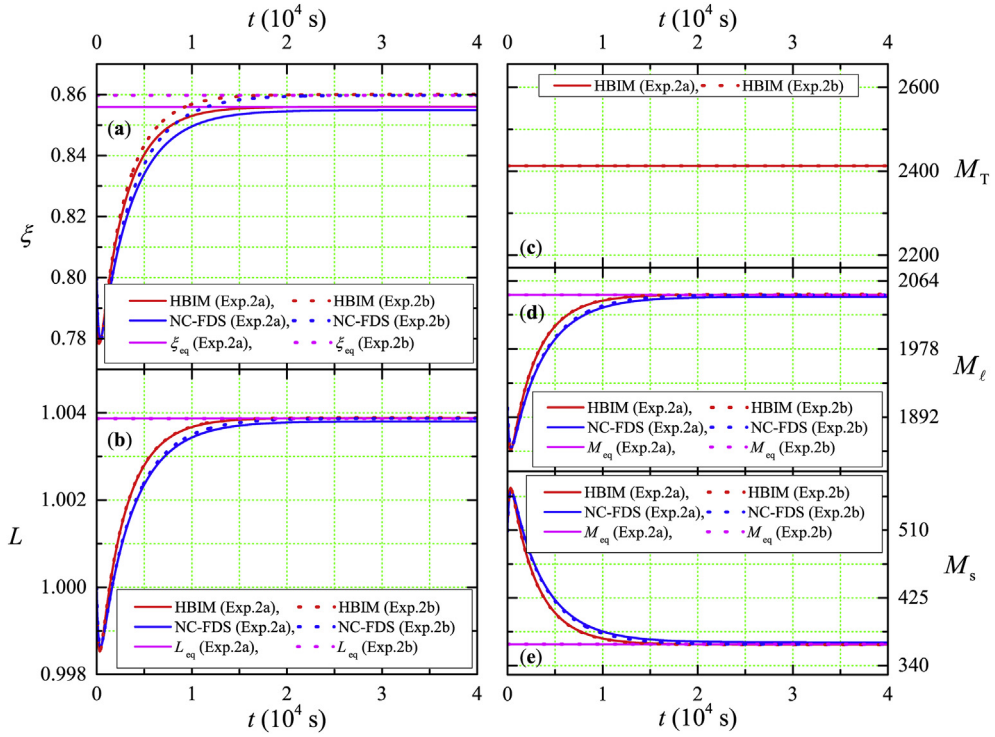

Fig. 8. Solutions for the constant mass model, corresponding to the example of Fig. 7. Time evolution calculated with the NC-FDS and HBIM along with the corresponding equilibrium values are shown for a) the interface position, b) sample size, c) total mass and d) liquid and e) solid masses. In solid lines, experiment 4a corresponds to a system where x_s is constant and x_ℓ is time dependent. In dotted lines, experiment 4b shows the results obtained from a system where x_s is the time-dependent boundary and x_ℓ is constant.

Table 2
Percent relative difference between the numerical values calculated with the HBIM and the NC-FDS at $t = 1 \times 10^4$ s, and exact values at thermodynamic equilibrium obtained from the example shown in Figs. 7 and 8. Percent relative differences were calculated as: $\left|(Y^{T}_{eq} - Y^{num}_{eq})/Y^{T}_{eq}\right| \times 100\%$.

Model	ξ^{T}_{eq}	ξ^{HBIM}_{eq}	ξ^{NC-FDS}_{eq}	HBIM Error	NC-FDS Error
	m	m	m	%	%
Constant Length	0.8558672	0.8612149	0.8608749	0.6248282	0.5851025
Constant Mass Exp. 2a	0.8558672	0.8559972	0.8548811	0.0151893	0.1152165
Constant Mass Exp. 2b	0.8597404	0.8600144	0.8597699	0.0318701	0.0034313
	$m^{T}_{\ell_{eq}}$	$m^{HBIM}_{\ell_{eq}}$	$m^{NC-FDS}_{\ell_{eq}}$	HBIM Error	NC-FDS Error
	kg	kg	kg	%	%
Constant Length	2036.9640	2049.6915	2048.8824	0.6248269	0.5851061
Constant Mass Exp. 2a	2046.1821	2046.5128	2043.6724	0.0161618	0.1226528
Constant Mass Exp. 2b	2046.1821	2046.8343	2046.2524	0.0318740	0.0034357
	$m^{T}_{s_{eq}}$	$m^{HBIM}_{s_{eq}}$	$m^{NC-FDS}_{s_{eq}}$	HBIM Error	NC-FDS Error
	kg	kg	kg	%	%
Constant Length	366.81793	353.20803	354.07327	3.7102603	3.4743831
Constant Mass Exp. 2a	366.81793	366.48724	369.32757	0.0901510	0.6841650
Constant Mass Exp. 2b	366.81793	366.16574	366.74757	0.1777967	0.0191812

- More general expressions for the asymptotic time behaviour of the interface were found and shown to depend on the frame of reference. These expressions describe the steady state regime for a system with isothermal boundary conditions, and they are observed to reproduce the result predicted when volumetric effects are neglected.
- Solutions from the general model, obtained through the NC-FDS and HBIM, capture the predicted behaviour of the interface position, system length and liquid and solid masses in the asymptotic time limit for a system with isothermal boundary conditions,
- Expressions for the interface position, system length, liquid and solid masses were also obtained for a system with adiabatic boundary conditions.
- It was shown that the asymptotic expressions found for system length and liquid and solid masses are independent of the frame of reference, and this was illustrated through the invariance of the numerical and semi-analytical solutions when moving the left or right boundary.
- The percentage error between the numerical solutions (NC-FDS and HBIM) for a system with adiabatic boundary conditions and the asymptotic values, was significantly reduced by using the

constant mass model. Two examples were used to illustrate how the relative error decreases for the constant mass model when compared with the classic Stefan model of a system with constant length.

References

[1] Zhou D, Zhao CY, Tian Y. Review on thermal energy storage with phase change materials (PCMs) in building applications. Appl Energy 2012;92:593–605. http://dx.doi.org/10.1016/j.apenergy.2011.08.025.

[2] Scalat S, et al. Full scale thermal testing of latent heat storage in wallboard. Sol Energy Mat Sol C 1996;44(1):49–61. http://dx.doi.org/10.1016/0927-0248(96)00017-7.

[3] Cabeza LF, Castellon C, Nogues M, Medrano M, Leppers R, Zubillaga O. Use of microencapsulated PCM in concrete walls for energy savings. Energy Build 2007;39(2):113–9. http://dx.doi.org/10.1016/j.enbuild.2006.03.030.

[4] Saman WY, Belusko M. Roof integrated unglazed transpired solar air heater. In: Lee T, editor. Proc. Of the 1997 australian and New Zealand solar energy society; 1997. Paper 66, Canberra, Australia.

[5] Vakilatojjar SM, Saman W. Analysis and modeling of a phase change storage system for air conditioning applications. Appl Therm Eng 2001;21(3):249–63. http://dx.doi.org/10.1016/S1359-4311(00)00037-5.

[6] Mathieu-Potvin F, Gosselin L. Thermal shielding of multilayer walls with phase change materials under different transient boundary conditions. Int J Therm Sci 2009;48(9):1707–17. http://dx.doi.org/10.1016/j.ijthermalsci.2009.01.010.

[7] Jesumathy SP, Udayakumar M, Suresh S. Heat transfer characteristics in latent heat storage system using paraffin wax. J Mech Sci Technol 2012;26(3):959–65. http://dx.doi.org/10.1007/s12206-011-1017-4.

[8] Akguna M, Aydna O, Kaygusuzb K. Experimental study on melting/solidification characteristics of a paraffin as PCM. Energy Convers manage 2007;48(2):669678. http://dx.doi.org/10.1016/j.enconman.2006.05.014.

[9] Lokesh S, et al. Melting/solidification characteristics of paraffin based nano-composite for thermal energy storage applications. Therm Sci 2015. http://dx.doi.org/10.2298/TSCI150612170L. Online First.

[10] Lamberg P. Approximate analytical model for two-phase solidification problem in a finned phase-change material storage. Appl Energy 2004;77(2):131–52. http://dx.doi.org/10.1016/S0306-2619(03)00106-5.

[11] Dutil Y, et al. A review on phase-change materials: mathematical modeling and simulations. Renew Sust Energy Rev 2011;15(1):112130. http://dx.doi.org/10.1016/j.rser.2010.06.011.

[12] Mazzeo D, et al. Analytical model for solidification and melting in a finite PCM in steady periodic regime. Int J Heat Mass Tran 2015;88:844861. http://dx.doi.org/10.1016/j.ijheatmasstransfer.2015.04.109.

[13] Pitie F, Zhao CY, Caceres G. Thermo-mechanical analysis of ceramic encapsulated phase-change-material (PCM) particles. Energy Environ Sci 2011;4:20117–2124. http://dx.doi.org/10.1039/C0EE00672F.

[14] Nomura T, et al. Microencapsulation of metal-based phase change material for high-temperature thermal energy storage. Sci Rep 2015;4:1–8. http://dx.doi.org/10.1038/srep09117.

[15] Wood AS, Mosally F, Al-Fhaid A. On high order polynomial heat balance integral implementations. Therm Sci 2009;13(2):11–25. http://dx.doi.org/10.2298/TSCI0902011W.

[16] Sadoun N, et al. On the goodman heat balance integral method for stefan like problems: further considerations and refinements. Therm Sci 2009;13(2):81–96. http://dx.doi.org/10.2298/TSCI0902081S.

[17] Ren He-Sheng. Application of the heat-balance integral to an inverse Stefan problem. Int J Therm Sci 2007;46(2):118–27. http://dx.doi.org/10.1016/j.ijthermalsci.2006.04.013.

[18] Mitchell SL, Myers TG. Application of standard and refined heat balance integral methods to one dimensional stefan problems. SIAM Rev 2010;52(1):57–86. http://dx.doi.org/10.1137/080733036.

[19] Yvonnet J, et al. The constrained natural element method (C-NEM) for treating thermal models involving moving interfaces. Int J Therm Sci 2005;44(6):559–69. http://dx.doi.org/10.1016/j.ijthermalsci.2004.12.007.

[20] Rajeev and Das S. A numerical study for inward solidification of a liquid contained in cylindrical and spherical vessel. Therm Sci 2010;14(2):365–72. http://dx.doi.org/10.2298/TSCI1002365R.

[21] Mackenzie JA, Robertson ML. The numerical solution of one-dimensional phase change problems using an adaptive moving mesh. J Comput Phys 2000;161:537–57. http://dx.doi.org/10.1006/jcph.2000.6511.

[22] Wu Zhao-Chun, Wand Qing-Cheng. Numerical approach to stefan problem in a two-region and limited space. Therm Sci 2012;16(5):1325–30. http://dx.doi.org/10.2298/TSCI1205325W.

[23] Mitchell SL, Vynnycky M. On the numerical solution of two-phase stefan problems with heat-flux boundary conditions. J Comput Appl Math 2014;264:49–64. http://dx.doi.org/10.1016/j.cam.2014.01.003.

[24] Javierre E, et al. Comparison of numerical models for one-dimensional stefan problems. J Comput Appl Math. 2006;192(2):445–59. http://dx.doi.org/10.1016/j.cam.2005.04.062.

[25] Dragomirescu FI, Eisenschmidt K, Rohde C, Weigand B. Perturbation solutions for the finite radially symmetric stefan problem. Int J Therm Sci 2016;104:386–95. http://dx.doi.org/10.1016/j.ijthermalsci.2016.01.019.

[26] Hernández EM, et al. Non parabolic interface motion for the one-dimensional stefan problem: dirichlet boundary conditions. Therm Sci 2016. http://dx.doi.org/10.2298/TSCI151114098H. Online-First.

[27] Otero JA, et al. Non parabolic interface motion for the one-dimensional stefan problem: neumann boundary conditions. Therm Sci 2016. http://dx.doi.org/10.2298/TSCI151218311O. Online-First.

[28] Mufu Y, Jihong Y, Bell T. Numerical simulation of nitrided layer growth and nitrogen distribution in ε -$Fe_{2-3}N$, $\gamma' - Fe_4N$ and $\alpha - Fe$ during pulse plasma nitriding of pure iron. Model Simul Mater Sci 2000;8(4):491–6. http://dx.doi.org/10.1088/0965-0393/8/4/307.

[29] Hernández EM, et al. Modeling of compound layer growth during nitriding of pure iron. Sci Res Essays 2016;11(13):135–46. DOI: 0.5897/SRE2016.6405.

[30] Danielewski M, et al. Chemical interdiffusion in binary systems; interface barriers and phase competition. J Appl Phys 2011;110:1–16. http://dx.doi.org/10.1063/1.3667293. 123705.